Volume 18, Number 4, 2025. pp. 477-488

Jordan Journal of Physics

ARTICLE

Effect of Annealing Temperature on the Properties of Cu_2ZnSnS_4 (CZTS) Thin Films for Solar Cell Application

Akintunde A. Ajayi[a], Aderemi B. Alabi[b], Enoch D. Ogunmola[a], Ayodeji O. Salau[c,g], Samson I. Akinsola[b], Olutayo W. Abodunrin[a], Olukunle C. Olawole[e], Folasade O. Oluyemi[d], Kazeem A. Musiliyu[a] and **Funmilayo H. Abejide[f]**

[a] *Department of Mathematical and Physical Sciences, Afe Babalola University, Ado-Ekiti, Nigeria.*

[b] *Department of Physics, University of Ilorin, Ilorin, Nigeria.*

[c] *Department of Electrical and Computer Engineering, Afe Babalola University, Ado-Ekiti, Nigeria.*

[d] *Department of Science Technology, Federal Polytechnic, Ado-Ekiti, Nigeria.*

[e] *Department of Physics, Covenant University, Ota, Nigeria.*

[f] *Department of Physics, Joseph Ayo Babalola University, Arakeji, Nigeria.*

[g] *Saveetha School of Engineering, Saveetha Institute of Medical and Technical Sciences, Chennai, Tamil Nadu, India.*

Doi: **https://doi.org/10.47011/18.4.6**

Received on: 16/06/2024; *Accepted on: 04/09/2024*

Abstract: In this paper, a CZTS precursor solution was prepared using ethylene glycol, and CZTS thin films were synthesized by spraying the solution on heated substrates. The effects of annealing temperature on structural, optical, and electrical properties of the sprayed CZTS thin films were studied. XRD studies revealed a wurtzite-structured CZTS thin film at an annealing temperature of 450 °C, while images obtained from SEM showed a homogeneous and agglomerated surface at the same temperature. UV-Vis spectroscopic studies revealed increasing absorbance with an increase in wavelength and a bandgap of 1.5 eV at 450 °C. Electrical studies showed the lowest resistivity at 450 °C, and a conversion efficiency of 0.12% was obtained from a spray-fabricated CZTS absorber-based thin-film solar cell with the configuration glass/ITO/i:ZnO/n:ZnS/p:CZTS/Ag.

Keywords: CZTS, Spray pyrolysis, Annealing, Structural properties, Optical properties, Electrical properties.

1. Introduction

Thin-film solar cells have been considered as alternatives to silicon-based solar cells because relatively fewer materials are required for their fabrication [1]. In a thin-film solar cell, sunlight generates electron-hole pairs in the semiconductor material. These pairs are separated by an electric field created by a junction or doping. Electrons are collected at the bottom electrode, while holes are collected at the top. The collected carriers flow through an external circuit, generating an electric current for powering devices or storage. It should be noted that although nanocrystalline silicon thin films, which can find applications in solar cells, have been developed [25], the abundance of silicon in the Earth's crust may be threatened by its present rate of consumption [26]. Some organic-inorganic hybrid nanomaterials have been explored as alternatives to silicon [27-29], but this class of semiconductor material suffers from

Corresponding Author: Akintunde Ayodeji Ajayi **Email**: ayodejiajayijp@gmail.com

instability in the form of degradation over time due to the interactions between the organic and inorganic components or environmental factors. Moreover, their synthesis is often complex, requiring precise control over the interactions between organic and inorganic components. Copper indium gallium selenide (CIGS) and cadmium telluride (CdTe) are thin-film solar cells that have achieved commercial success. However, the indium constituent in CIGS is a rare earth element and, as a consequence, has a negative impact on the affordability of CIGS solar cells. At the same time, cadmium's carcinogenic nature raises concerns about the environmental and health effects of decommissioned CdTe solar cells [3]. Copper zinc tin sulfide (CZTS) is a suitable alternative due to the abundance of copper, zinc, tin, and sulfur in the Earth's crust. CZTS has a high absorption coefficient ($> 10^{-4}$ cm^{-1}) and a direct bandgap of 1.5 eV [4]. The theoretical conversion efficiency of the CZTS absorber-based solar cell has been calculated to be above 30%. Highly efficient CZTS absorber-based solar cells have been created through physical techniques. Nevertheless, the inclusion of vacuum equipment in this deposition process raises the market cost of the final product in the event of commercialization [5, 6].

Chemical or solution-based techniques are alternatives to physical techniques in terms of cost. The most successful CZTS solar cells to date have typically employed cadmium sulfide (CdS) as the n-type junction material or incorporated cadmium into the absorber layer [7], and a solution other than water has been used as a solvent in the case of a solution-based fabrication process. The CZTS solar cell with the present highest efficiency (12.6%) was fabricated using a solution-based technique with hydrazine employed as the solvent [8]. Hydrazine is an explosive and toxic material, and its use in commercial fabrication of CZTS solar cells will lead to extra costs due to stringent safety and handling requirements [9]. Developing a cadmium-free CZTS solar cell using both physical and chemical techniques can be challenging in terms of cost and safety. Patel and Gohel [10] investigated the effects of different solvents on the properties of CZTS thin films and found that films synthesized using ethylene glycol and propylene glycol exhibited superior characteristics. Recent studies on the influence of annealing temperature on CZTS thin films have shown that their structural, optical, morphological, and electrical properties improve with increasing annealing temperatures between 250 °C and 550 °C. Olgar *et al*. [11] synthesized CZTS thin films via magnetron sputtering and reported enhanced film properties, achieving optimal solar cell performance at 550 °C. Electrical and back-contact studies of metal/CZTS/ZnS/ZnO/FTO heterojunction devices fabricated by spray pyrolysis were conducted by Boutebakh *et al*. [36]. Their results revealed rectifying behavior in CZTS/ZnS structures for all tested back contacts, with gold (Au) exhibiting the best rectification and the highest ideality factor. These findings highlight the strong potential for developing cadmium-free CZTS-based devices capable of efficient power generation. This research addresses a significant gap in current knowledge regarding the synthesis and characterization of copper zinc tin sulfide (CZTS) thin films for solar cell applications. Despite the promising attributes of CZTS, comprehensive studies on the combined effects of solvent choice, annealing temperature, and the resulting structural, optical, morphological, and electrical properties of CZTS thin films prepared by spray pyrolysis are limited.

In our study, we utilized ethylene glycol as a solvent to synthesize CZTS thin films via spray pyrolysis and systematically examined the effects of annealing temperature on their structural, optical, morphological, and electrical properties. Our objective was to enhance understanding of how synthesis parameters influence CZTS thin-film solar cell performance, with particular emphasis on achieving improved efficiency and device characteristics for cadmium-free CZTS absorber-based solar cells.

The major contributions of this paper are summarized as follows:

i. **Methodological Advancement**: We employed ethylene glycol as a solvent for CZTS thin-film synthesis, providing a cost-effective and environmentally friendly alternative to conventional solvents. The deposition technique used is simple, scalable, and economical. Furthermore, our systematic investigation of annealing temperatures offers valuable insights into optimizing the fabrication process of CZTS thin-film solar cells.

ii. **Practical Implications**: The insights gained from our research can inform the

development of more efficient and affordable CZTS thin-film solar cells, thereby supporting the advancement of renewable energy technologies. By elucidating the relationships between synthesis parameters and material properties, this work lays the foundation for future research aimed at the commercialization of CZTS-based photovoltaic devices.

2. Materials and Methods

A precursor solution containing 0.035 M copper, 0.025 M zinc, 0.025 M tin, and 0.2 M sulfur salts was prepared for deposition on thoroughly cleaned substrates. The precursor salts used in preparing the CZTS solution are copper (II) acetate ($C_4H_6CuO_4$), zinc acetate dihydrate ($Zn(CH_3CO_2)_2.2H2O$, tin (IV) chloride pentahydrate ($SnCl_2.5H_2O$), and thiourea ($SC(NH_2)_2$), serving as the sources of copper, zinc, tin, and sulfur, respectively. A precursor of 0.015 M copper acetate was also prepared. The solvents used are deionized water and ethane-1,2-diol ($(CH_2OH)_2$), also known as ethylene glycol. All reagents were analytical grade and purchased from Sigma-Aldrich. The as-prepared precursor mixture was stirred for 1 hour using a magnetic stirrer. The concentration of thiourea was higher in order to maintain stochiometry and compensate for the loss of sulfur during pyrolysis. The CZTS precursor solution was deposited on clean glass and indium tin oxide (ITO) substrates using the spray pyrolysis technique, with the substrate surface maintained at 350 °C. The resulting CZTS thin films were annealed in a muffle furnace at temperatures of 250 °C, 350 °C, and 450 °C, and labeled samples A25, A35, and A45, respectively.

A heterojunction solar cell was fabricated using optimized CZTS and ZnS thin-film layers. A glass/ITO/iZnO/n-ZnS/p-CZTS/Ag solar cell configuration was employed in the layering process. The zinc oxide anti-reflective window layer was synthesized by spraying zinc acetate solution onto ITO-coated glass substrates in open air and annealed at 350 °C for 1 hour. This was followed by the spraying of ZnS precursor solution on the annealed ZnO anti-reflective layer and annealing of the ZnS layer at 350 °C. The p-CZTS thin-film layer was obtained by spraying the CZTS precursor onto the annealed n-ZnS layer. The p-CZTS layer was annealed at 450 °C. Silver (Ag) was used as the back contact for the cell. Colloidal silver was purchased from Sigma-Aldrich.

The structural characterization of the specimens was carried out with the aid of a Rigaku D/Max-IIIC x-ray diffractometer with a LynxEye detector using a copper target (Cuα,1.5418 Å). All x-ray diffraction (XRD) data for the samples were recorded at current and acceleration voltages of 25mA and 40 kV, respectively. Morphological and grain growth analysis of the specimen was carried out by using a Hitachi scanning electron microscope (SEM), and optical characterization was done using a CyberLab UV-vis spectrophotometer (model UV-100). Film thickness measurements were carried out using a Veeco Dektak surface profilometer. The chemical composition of the samples was studied using the energy dispersive X-ray (EDX) analysis method. Electrical characterization was carried out using the four-point probe method. The equipment employed was a Holmarc solar simulator and a Keithley source meter (Model HO-SCIVK) with indium used as the ohmic contact and with a 300 W xenon lamp. The same Keithley source meter was used to determine the current-voltage (I-V) characteristics of fabricated solar cell devices. The devices were illuminated under strong white light.

3. Results and Discussion

3.1 Structural Properties

The XRD pattern of A-25 is shown in Fig. 1, where diffraction peaks of kesterite CZTS can be observed at 2θ values of 23.00^0, 42.90^0, and 76.29^0, which can be indexed to (110), (200), and (332) reflection planes (JCPDS 26-0575). Secondary phases that can be indexed to the hexagonal plane of ZnS at $2\theta = 48.2^0$ and also ZnO at $2\theta = 67.30^0$ were observed.

The XRD pattern of A35 is shown in Fig. 2. Diffraction peaks of wurzite-phased CZTS corresponding to (100), (202), (220), and (008) reflection planes can be seen at 26.50^0, 37.35^0, 47.54^0, and 69.43^0, which are respective values of 2θ. There is no standard JCPDS card for wurzite CZTS. The crystal structure of wurtzite Cu_2ZnSnS_4 (CZTS) can be derived by substituting Zn(II) ions with Cu(I), while maintaining the Zn(II) and Sn(IV) positions in the wurtzite ZnS structure. In this structure, each sulfur ion is coordinated with two Cu(I) ions,

one Zn(II) ion, and one Sn(IV) ion, satisfying the octet rule [(8/4)+6=8]. It's important to note that in this model, the distribution of metal cations occurs randomly within the fixed framework formed by sulfur anions. Consequently, the XRD pattern of wurtzite CZTS remains largely similar to that of wurtzite ZnS [12]. Peaks corresponding to ZnS and ZnO impurities can be observed at 2θ equals 30.2^0 and 62.60^0, respectively. The XRD of A45 is shown in Fig. 3 with diffraction peaks at 2θ equals 26.97°, 37.41°, 47.50°, 69.81°, and 76.50°, which can be indexed to the (100), (202), (220), (008), and (332) reflection planes of wurzite-phased CZTS. While the solvent may have indirectly influenced the annealing process kinetics, the crystal structure phase transition from kesterite to wurzite is likely attributed to faster crystal growth facilitated by high thermal energy. These results are in agreement with Lu *et al.* [12] and Touati *et al.* [13]. The higher peak intensity observed in sample A25 may be due to the presence of a larger number of smaller crystallites in the film annealed at 250 °C. These small grains can contribute to a higher number of diffracting planes that align with the X-ray beam. As the annealing temperature increases, the additional thermal energy promotes grain growth and reorganization. Larger grains may form, leading to fewer grain boundaries and a more ordered crystalline structure. However, fewer grains align in the optimal orientation for diffraction, leading to a decrease in peak intensity. The crystallite sizes were calculated from the FWHM of the (110) orientation for sample A25 and (110) for A35 and A45. The crystallite sizes were 13.46 nm, 21.46 nm, and 45.10 nm. The results indicated that a better crystallinity is obtained at an annealing temperature of 450 °C. The crystallite sizes were calculated using Eq. (1):

$$D = \frac{0.9\lambda}{\beta\cos\theta} \quad (1)$$

where λ is the wavelength of the used X-ray beam (1.54 Å), β is the full width at half maximum, and θ is the angle of diffraction. The microstructural strain (ε) is calculated using Eq. (2), and the values obtained at different annealing temperatures are shown in Tables 1, 2, and 3.

$$\varepsilon = \frac{\beta cos\theta}{4} \quad (2)$$

Thermal expansion of CZTS thin films and substrates upon heat treatment can be correlated to strain in the films [12]. Calculation of strain for annealed CZTS thin films showed a reduction with an increase in annealing temperature. Dislocation density, which is the measure of linear crystallographic defects within the crystal structure, was calculated for annealed CZTS films using Eq. (3).

$$\delta = \frac{n}{D^2} \quad (3)$$

where D is the crystallite size and n is unity when the dislocation density is minimum. The values of the microstructural strain and dislocation density are shown in Table 1. The lowest microstructural strain can be observed in specimen A45.

TABLE 1. Details of the structural analysis of annealed CZTS thin film specimens.

Specimen	Crystallite Size (nm)	Micro strain (ε) x 10^{-3}	Dislocation density δ (lines/m^2) x 10^{15}
A25	13.46	2.77	5.52
A35	21.46	1.61	2.17
A45	45.10	0.78	0.49

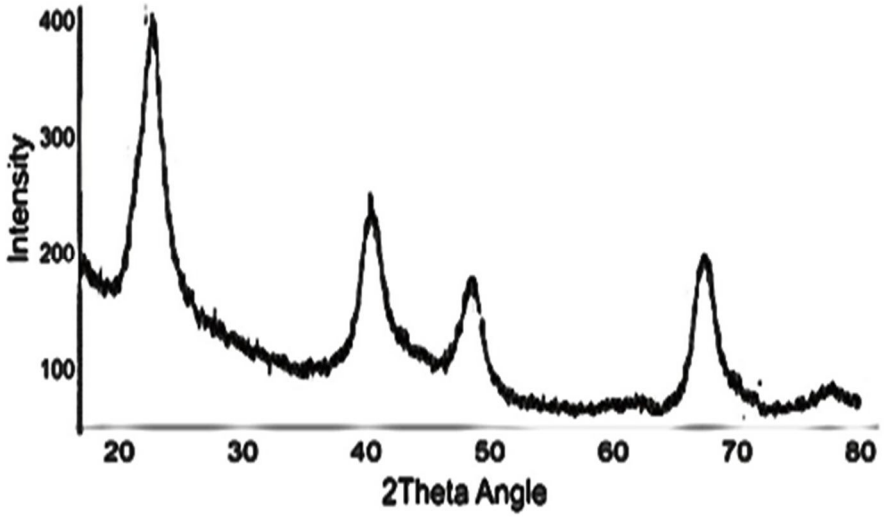

FIG. 1. X-ray diffraction pattern of CZTS thin films annealed at 250 °C (specimen A25).

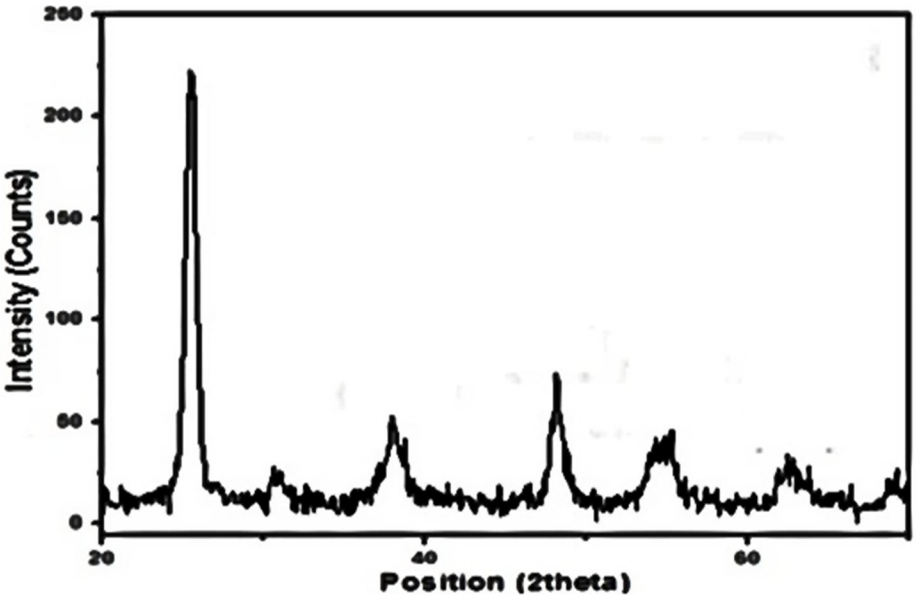

FIG. 2. X-ray diffraction pattern of CZTS thin films annealed at 350 °C (specimen A35).

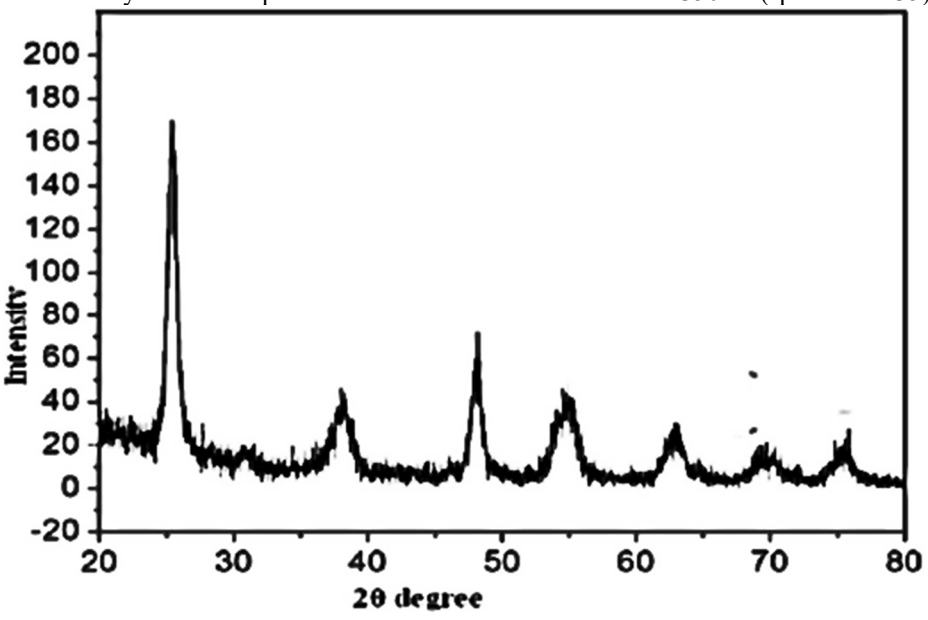

FIG. 3. X-ray diffraction pattern of CZTS thin films annealed at 450 °C (specimen A45).

3.2 Optical Properties

Figures 4 and 5 show the plots of the absorbance and transmittance versus wavelength. The highest absorbance and the lowest transmittance within the ultraviolet-visible region can be observed in A35 and A45, although the absorbance of A45 surpasses that of A35 around 550 nm wavelength. Phase change from kesterite to wurzite at 450 °C and surface roughness at that temperature may have been responsible for the increase in absorbance of A45 with increasing wavelength. The lowest absorbance and highest transmittance can be observed in A25. A good solar cell absorber material must have higher absorbance and low transmittance, and these results have demonstrated that a very efficient CZTS absorber material can be obtained at annealing temperatures of 350 °C and 450 °C. The Tauc plots are shown in Fig. 6 for A25, A35, and A45. It can be observed from the $(\alpha hf)^2$ versus hf plot that the band gap values of CZTS thin films decrease with annealing temperature. A45 has a band gap of 1.48 eV, which is almost equal to the ideal band gap of CZTS, while band gaps of 1.80 eV and 1.93 eV were obtained for A35 and A25, respectively. These results are in agreement with recent works [14, 15]. An explanation for the decrease in band gap with increasing annealing temperature in A45 is the quantum confinement effect. Quantum confinement effect is observed when crystallite size is approaching the de Broglie wavelength of an electron, and an increase in band gap has been correlated to greater quantum confinement of the grains [14].

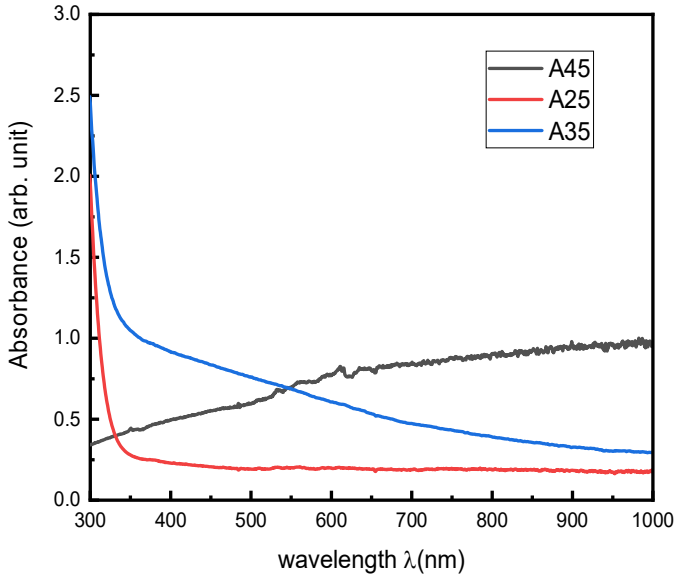

FIG. 4. Absorbance spectra of CZTS thin films with annealing temperatures.

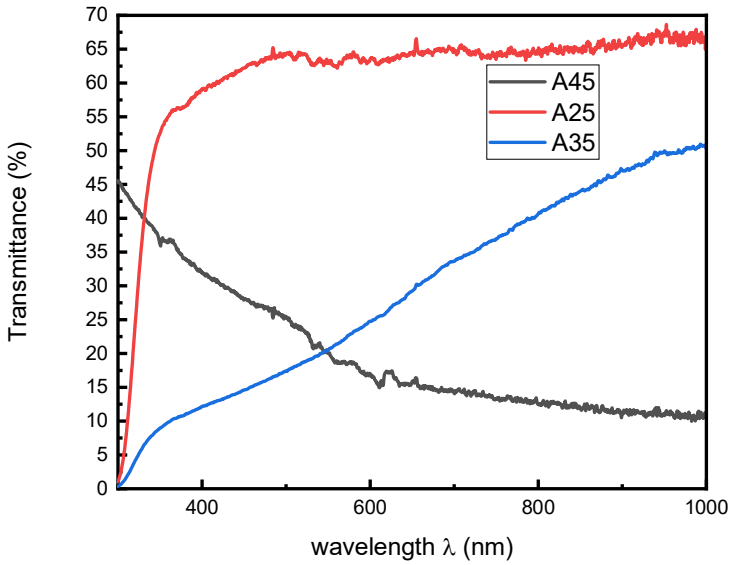

FIG. 5. Transmittance spectra of CZTS thin films with annealing temperatures.

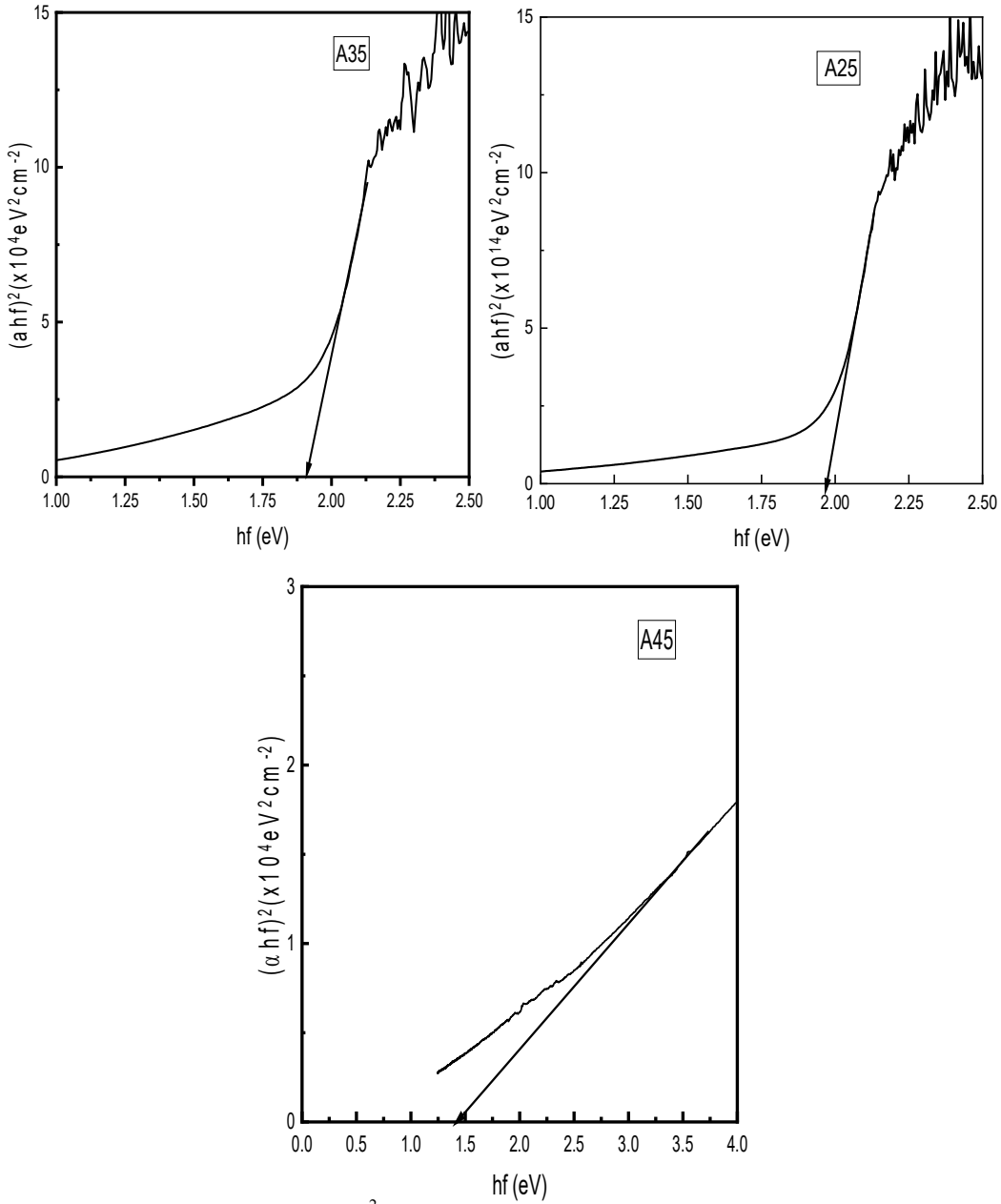

FIG. 6. Plot of $(\alpha hf)^2$ versus hf for specimens A25, A35, and A45.

3.3 Surface Morphology

The top-down SEM images of A45, A35, and A25 are shown in Figs. 7(a), 7(b), and 7(c), respectively. The increase in size of crystals in response to increasing annealing temperatures can be observed from the micrographs. These results are in agreement with previous works [16, 17]. Large voids and small crystallites with sizes below 500 nm are evident in A25. The voids observed on the surface of A25 can be attributed to the presence of an amorphous carbon layer formed beneath the thin film that did not completely evaporate during the annealing process. Upon increasing the annealing temperature to 350 °C, a reduction in voids and an increase in crystallite size were observed, although the surface morphology remained nonhomogeneous. Large crystals, which are undefined with distinct grain boundaries, can also be observed in A35, with some of the crystals having sizes greater than 2 micrometers. It has been reported that grain boundaries reduce minority carrier diffusion, which is detrimental to solar cell performance [18]. Superior surface morphology can be observed at an annealing temperature of 450 °C, with voids almost completely absent, with improved compactness and homogeneity.

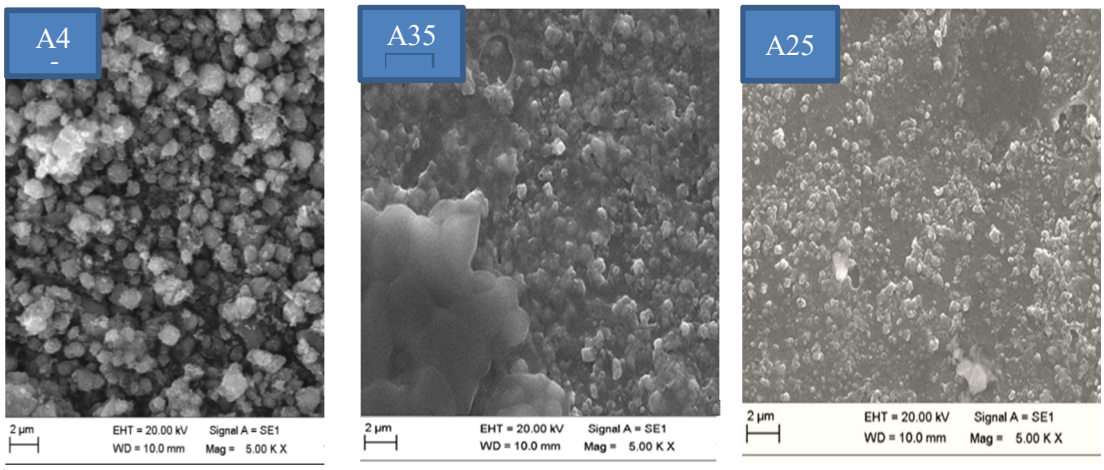

(a) (b) (c)

FIG. 7. SEM of CZTS thin film for specimens (a) A25, (b) A35, and (c) A45.

3.4 Analysis of the Composition of CZTS Thin Films Annealed at 450 °C

The EDX spectrum of A45 is shown in Fig. 8. The presence of copper, zinc, tin, and sulfur peaks in the EDX spectra confirms the composition of the CZTS compound in the A45 sample. However, it is noteworthy that all the films exhibit significant sulfur deficiency, which can be attributed to the tendency of sulfur to react with oxygen and form sulfur dioxide (SO_2), which is subsequently lost during the pyrolysis process. High percentages of carbon and oxygen seen in the spectra may not be solely as a result of oxidation of the specimen

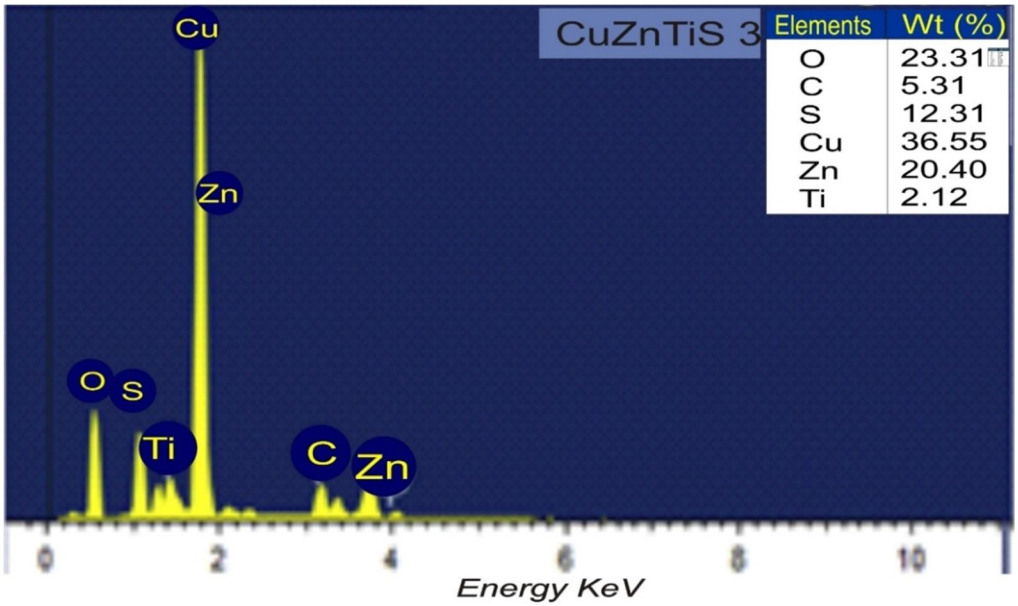

FIG. 8. EDX spectrum of A45.

3.5 Electrical Properties

The electrical properties of sprayed CZTS thin films were studied at different annealing temperatures. The resistivity of the films was obtained using Eq. (4):

$$\rho = \left(\frac{V}{I}\right)\frac{A}{L} \quad (4)$$

where V is the voltage measured across the outer probes, I is the current passing through the inner probes, A is the cross-sectional area of the CZTS thin film specimen, and L is the distance between the inner probes. The resistivity of annealed CZTS thin films is shown in Table 2. It can be observed that resistivity decreases with an increase in annealing temperature. The results show that better electrical properties can be obtained at an annealing temperature of 450 °C and are in agreement with previous works in the literature [19]. An explanation for the high resistivity of CZTS thin film annealed at 250 °C is the high microstructural strain in the films,

which can be observed in Table 1. Theoretical calculations and experimental studies have shown that strain in films is due to inhomogeneity in composition, which in turn alters the shape of the valence bands [20]. In other words, strain can be induced by secondary phases apart from the strain stemming from the film fabrication process. The result is a negative impact on hole carrier transport and electron-hole recombination at the junction. It can also be argued that high resistivity at low annealing temperatures is due to the presence of undecomposed organic residuals in the CZTS thin film. The lowest resistivity was calculated for CZTS thin film annealed at 450 °C, with the lowest micro-structural strain shown in Table 1. The electrical conductivity of CZTS films is improved at an annealing temperature of 450 °C.

TABLE 2. Electrical resistivity of CZTS thin films annealed at different temperatures.

Specimen	Sheet Resistance (Ω/sq) (x 10^7)	Resistivity (Ωcm) (x 10^{-1})	Thickness (nm)
A25	1.60	2.59	1625
A35	1.10	1.71	1620
A45	8.79	0.71	1621

3.6 Characterization of Glass/ITO/i:ZnO/n:ZnS/ p:CZTS/Ag Solar Cell

Glass/ITO/i:ZnO/n:ZnS/p:CZTS/Ag solar cells were fabricated at the optimized annealing temperature parameter that has shown the best properties for the absorber layer using the spray pyrolysis technique. The I-V characteristics of the cell, taken in the dark and under illumination, are shown in Fig. 9, where a rectifying curve with low reverse saturation current can be observed. This is evidence that the junction between CZTS and ZnS has diode characteristics, with the possibility of the production of an electron-hole pair when the heterojunction is under illumination. The results are in agreement with the work of Patel *et al.* [23] and Fathima *et al.* [24], which have exhibited comparable rectifying curves for FTO/Al:ZnO/CdS/CZTS/CuS/FTO and FTO/Ag/CdS/Ag solar cell architectures, respectively. The photocurrent output was obtained from Eq. (5).

$$\eta = \frac{P_{max}}{P_{in}} = \frac{FFV_{oc}I_{sc}}{P_{in}} \quad (5)$$

where FF is the fill factor, V_{OC} is the open circuit voltage, and I_{SC} is the short circuit current. P_{max} is the maximum power that can be delivered by the solar cell. P_{in} was calibrated to AM 1.5 to 100 mW/cm^{-2} before measurements were carried out. The photocurrent output of the cell was extremely low, with the short circuit current calculated to be 0.022 mA, and the efficiency of the cell was less than 0.1%. The low performance of the cell may be attributed to secondary phases that may have similar XRD peaks to CZTS. Since the formation of single-phase CZTS can be very challenging, ZnS and Cu_2SnS_3 (CTS) phases that have the same XRD patterns as CZTS will go undetected [21, 22]. Since ZnS was suspected to be the culprit, the CZTS absorber layer was etched with 0.1 M of HNO_3 for the removal of the ZnS phase by immersing the synthesized CZTS thin film in HNO_3 for 300 seconds. The decomposition of ZnS is represented by Eq. (6).

$$HNO_3 + ZnS \rightarrow H_2O + S + NO + Zn(NO_3)_2 \quad (6)$$

Another CZTS solar cell with the same solar architecture as the first was fabricated using the etched CZTS as an absorber layer, and the I-V characteristics of the cell, taken in the dark and under illumination, are shown in Fig. 9(a) and Fig. 9(b), respectively, while those with the HNO_3- etched CZTS layer in the dark and under illumination are shown in Fig. 10. After etching, the photocurrent increased to 0.258 mA, with a corresponding conversion efficiency of 0.13%. The wurtzite phase of the CZTS thin film annealed at 450 °C may have contributed to reduced recombination losses by providing efficient pathways for charge carriers to reach the electrodes. A summary of the I–V parameters of the fabricated solar cells is presented in Table 3. Recent literature on CZTS thin-film solar cells is summarized in Table 4. Comparison shows that the open-circuit voltage and photocurrent output of our cells are lower than those reported in literature; however, most high-performance CZTS cells involve cadmium. Moreover, some studies [30,31,37,38] incorporate germanium, which is expensive due to the high cost of achieving 99.9% purity. In contrast, our work demonstrates a simple, scalable, and environmentally friendly fabrication method using earth-abundant, low-cost, and safe materials.

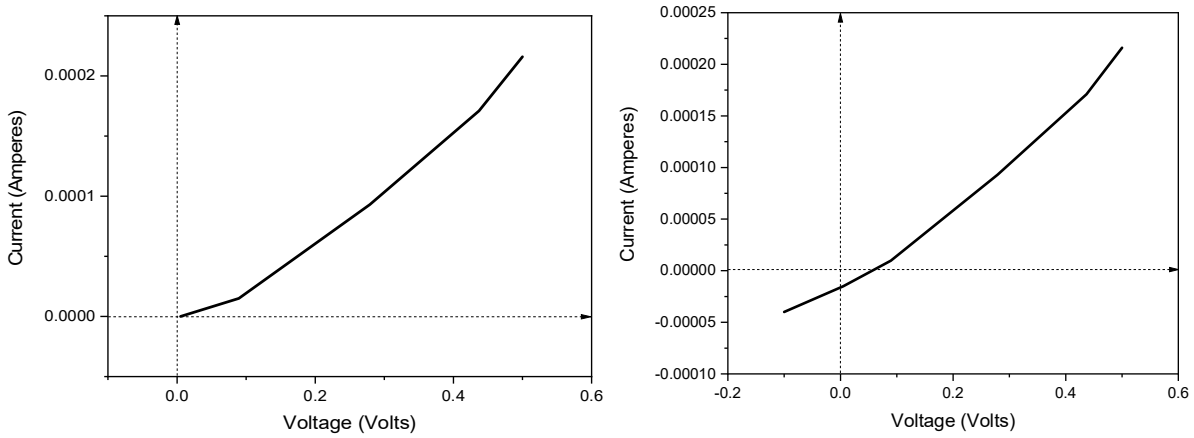

(a) (b)

FIG. 9. I-V characteristics of ITO/i:ZnO/n:ZnS/p:CZTS/Ag thin film solar cell in the dark and under illumination.

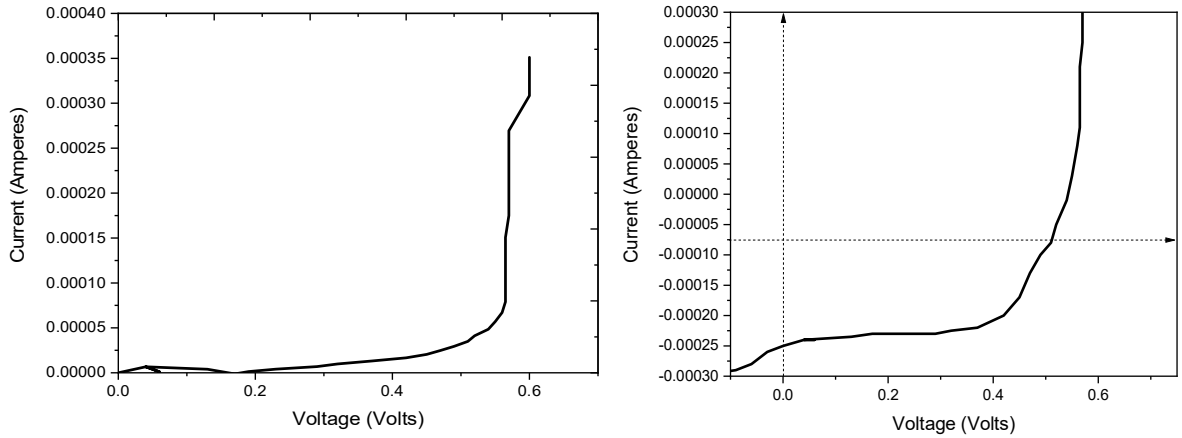

FIG. 10. I-V characteristics of ITO/i:ZnO/n:ZnS/p:CZTS/Ag thin film solar cell with HNO_3- etched CZTS layer in the dark and under illumination.

TABLE 3. Summary of the I-V characteristics of the fabricated CZTS absorber-based solar cells under illumination.

Device	Area of cell (cm^2)	V_{oc} (volts)	I_{sc} (mA)	V_{max} (volts)	I_{max} (mA)	Fill Factor	Efficiency (%)
ITO/i:ZnO/n:ZnS/p:CZTS/Ag	2.50 x 2.50	0.06	0.05	0.02	0.01	0.15	2.88×10^{-5}
ITO/i:ZnO/n:ZnS/p:CZTS/Ag (etched with HNO_3)	2.50 x 2.50	0.54	0.26	0.40	0.20	0.57	0.12

TABLE 4. Recent references on CZTS buffer layers.

CZTS Buffer Layer	Solar Cell Structure	Efficiency (%)	Deposition Method	J_{sc} (mA/cm^2)	Fill Factor	V_{oc}(mV)	Reference
Ge (alloyed with CZTS)	CZTS/Ge (followed by Sulphurization)	10.7	Sputtering	21.0	63.70	800	[30]
CdS+Salvia dye	SLG/Mo/CZTS/CdS/ ZnO/AZO	0.27	Sputtering	8.54	0.29	107.0	[31]
ZnSnO	SLG/Mo/CZTS/ZTO	9.3	Atomic Layer Deposition	21.00	65.8	736	[38]
CdS/TiO_2	SLG/Mo/CZTS/TiO_2/ AZO	3.59	Sputtering and Plasma	13.8	31.0	347	[37]

4. Conclusion

This paper presented the synthesis of CZTS thin films via the chemical spray pyrolysis technique. The effects of annealing temperature on the structural, optical, and electrical properties of the synthesized films were studied broadly. The results show the growth of the wurzite crystal structure for CZTS thin film annealed at higher temperatures. The largest grain size and lowest microstructural strain were obtained at 450 °C. SEM images showed that a more homogenous and void-free surface was obtained at 450 °C. The optical properties are widely affected by variation in annealing temperature. An increase in absorbance and a decrease in transmittance with increasing wavelength were observed at 450 °C, and a bandgap closer to the ideal bandgap of 1.5 eV was obtained. The CZTS thin film annealed at 450 °C indicated the lowest resistivity. A solar cell was fabricated with ZnS as an n-type partner, and a conversion efficiency of 0.12% was achieved.

Funding: The authors declare no funding for this research

Competing interests: The authors declare that they have no competing interests

Conflicts of interest: The authors declare that they have no conflicts of interest

Availability of data: The datasets generated during and/or analyzed during the current study are not publicly available but are available from the corresponding author on reasonable request.

Ethical Approval: Not applicable

Code availability: Not applicable

Acknowledgments: Not applicable

References

[1] Zhang, X. et al., Sci. Rep., 8 (248) (2018) 1.

[2] Zhu, R., Zhang, Z., and Li, Y., Nanotechnol. Rev., 8 (1) (2019) 452.

[3] Zappetini, A., Woodhead Publ. Ser. Electro. Opt. Mater., 2019 (2019) 273.

[4] Pal, K., Singh, P., Bhaduri, A., and Thapa, K.B., Sol. Energy Mater. Sol. Cells, 196 (2019) 138.

[5] Boersu, I. and Vasile, B.G., Materials, 15 (23) (2023) 1.

[6] Sah, M., Reddy, V.R.M, Kim, B., Patro, B., Kim, W.K., and Sharma, P., Mater., 15 (5) (2022) 6.

[7] Yan, C. et al., Nat. Energy, 3 (2018) 764.

[8] Wang. W. et al., Adv. Energy Mater., 4 (7) (2014) 1.

[9] Faremi, A.A. et al., Results Eng., 16 (2022) 100622.

[10] Patel, S.B. and Gohel, J.V., Phys. Astron. Int. J., 1 (4) (2017) 1.

[11] Olga, M.A., Sarp, A.O., Seyhan, A., and Zan, R., Renew. Energy, 179 (2021) 1865.

[12] Lu, X., Zhuang, Z., Penq, Q., and Li, Y., Chem. Commun., 47 (2011) 3141.

[13] Touati, R., Rabeh, M.B., and Kanzari, M., Energy Procedia., 44 (2014) 44.

[14] Chalapathi, U., Poornaprakash, B., and Park, S.H., Chalcogenide Lett., 15 (10) (2018) 475.

[15] Rey, G. et al., Appl. Phys. Lett., 105 (2014) 1.

[16] Izadneshan, H. and Solookinejad, G., J. Optoelectron. Nanostruct., 3 (2) (2018) 20.

[17] Singh, T., Pandya, D.K., and Singh, R., Mater. Chem. Phys., 130 (3) (2011) 1366.

[18] Raiguru, J. et al., Mater. Sci. Eng., 178 (2017) 1.

[19] Chen, L. and Park, C., Korean J. Chem. Eng., 34 (4) (2017) 1187.

[20] Patel, S.B. and Gohel, V.J., Phys. Astron. Int. J., 1 (4) (2017) 126.

[21] Syafiq, U., Ataolahhi, N., Maggio, R., and Scardi, P., Molecules, 24 (2019) 3454.

[22] Chalapathi, U., Poornaprakash, B., and Park, S., Chalcogenide Lett., 15 (10) (2018) 475.

[23] Patel, S.B. and Gohel, V.J., J. Mater. Sci. Mater. Electron, 29 (2018) 5613.

[24] Fathima, M.I., Arulamantham, A.M., and Wilson, K.S., Mater. Res. Express., 7 (2020) 1.

[25] Tripathi, R.K., Panwar, O.S., Rawal, I., Singh, B.P., and Yadav, B.C., J. Taiwan Inst. Chem. Eng., 86 (2018) 185.

[26] Franco, M.A. and Groesser, S.N., Sustainability, 13 (17) (2021) 1.

[27] Rawal, I., Tripathi, R.K., and Panwar, O.S., RSC Adv., 6 (37) (2016) 31540.

[28] Tripathi, R.K. et al., RSC Adv., 4 (97) (2014) 54388.

[29] Rawal, I., Dwivedi, N., Tripathi, R.K., Panwar, O.S., and Malik, H.K., Mater. Chem. Phys., 202 (2017) 169.

[30] Wang, A. et al., Adv. Mater., 36 (2024) 1.

[31] Najim, A.S. et al., Sci. Rep., 13 (1) (2023) 1.

[32] Orelusi, A.N., Owoeye, V.A., Dada, J.B., Salau, A.O., Boyo, H.O., and Adewinbi, S.A., J. Mater. Res., 38 (2023) 4192.

[33] Faremi, A.A., Olubambi, P.A., Salau, A.O., and Ibiyemi, A.A., Results Eng., 18 (2023) 1.

[34] Faremi, A.A., Olubosede, O., Salau, A.O., Adigbo, S.O., Olubambi, P.A., and Lawan, E., Mater. Renew. Sustain. Energy., 12 (3) (2023) 235.

[35] Salau, A.O., Olufemi, A.S., Oluleye, G., Owoeye, V.A., and Ismail, I., Mater. Today, 51 (1) (2022) 502.

[36] Boutebakh, F.Z., Zeggar, M.L., Attaf, N., and Aida, M.S., Optik, 144 (2017) 180.

[37] Tseberlidis, G., Barchiesi, E., Colombo, A., and Fabrizio, M., Eur. J. Inorg. Chem., 2023 (7) (2023) 703.

[38] Cui, X., Sun, K., Huang, J., Lee, C.-Y., Yan, C., Sun, H., Zhang, Y., Liu, F., Hossain, Md. A., Zakaria, Y., Wong, L.H., Green, M., Hoex, B., Hao, X., Chem. Mater., 30 (2018) 7860.